



# The Aneto Glacier (Central Pyrenees) evolution from 1981 to 2022: ice loss observed from historic aerial image photogrammetry and recent remote sensing techniques

Ixeia Vidaller<sup>1</sup>, Eñaut Izagirre<sup>2</sup>, Luis Mariano del Rio<sup>3</sup>, Esteban Alonso-González<sup>4</sup>, Francisco Rojas-Heredia<sup>1</sup>, Enrique Serrano<sup>5</sup>, Ana Moreno<sup>1</sup>, Juan Ignacio López-Moreno<sup>1</sup>, Jesús Revuelto<sup>1</sup>

<sup>1</sup> Instituto Pirenaico de Ecología, Consejo Superior de Investigaciones Científicas (IPE-CSIC), Zaragoza, Spain

<sup>2</sup> Department of Geography, Prehistory and Archaeology, University of the Basque Country UPV/EHU, Vitoria-Gasteiz, Spain

<sup>3</sup> Department of Applied Physics, Escuela Politécnica Superior de Cáceres, University of Extremadura, Cáceres, Spain

<sup>4</sup> Centre d'Etudes Spatiales de la Biosphère, Université de Toulouse, CNRS/CNES/IRD/INRA/UPS, Toulouse, France

10 <sup>5</sup> Department of Geography, GIR PANGAEA, University of Valladolid, Valladolid, Spain

15 *Corresponding author:* Ixeia Vidaller (ixeia@ipe.csic.es)

Abstract. The Aneto Glacier, although it may be considered very small (<0.5 km<sup>2</sup>), is the largest glacier in the Pyrenees. Its shrinkage and wastage have been continuous in recent decades, and there are signs of accelerated melting in recent years. In this study, changes in the area and volume of the Aneto Glacier from 1981 to 2022 are investigated using historical aerial imagery, airborne LiDAR point clouds, and UAV imagery. A GPR survey conducted in 2020, combined with data from photogrammetric analyses, allowed us to reconstruct the current ice thickness and also the existing ice distribution in 1981 and 2011. Over the last 41 years, the total glaciated area has shrunk by 64.7% and the ice thickness has decreased, on average, by 30.5 m. The mean remaining ice thickness in autumn 2022 was 11.9 m, as against the mean thicknesses of 32.9 m, 19.2 m and 15.0 m reconstructed for 1981 and 2011 and observed in 2020 respectively. The results demonstrate the critical situation of the glacier, with an imminent segmentation into two smaller ice bodies and no evidence of an accumulation zone. We also found that the occurrence of an extremely hot and dry year, as observed in the 2021–2022 season, leads to a drastic degradation of the glacier, posing a high risk to the persistence of the Aneto Glacier, a situation that could extend to the rest of the Pyrenean glaciers in a relatively short time.

Keywords: Aneto Glacier, Pyrenees, LiDAR, Unmanned Aerial Vehicle (UAV), Historical Aerial Images, Ground Penetrating Radar (GPR)



## 1 Introduction

Glaciers are excellent indicators of climate variability and change because their evolution depends on the balance between snow accumulation during the cold period and ice/snow ablation during the warmest season (Braithwaite and Hughes, 2020). The Little Ice Age (LIA) represents the last cold pulse in almost all mountain ranges of the world (Solomina et al., 2016; 35 García-Ruiz et al., 2020). As Grove (2004) and Oliva et al. (2018) point out, the LIA in the Pyrenees occurred during the period between the 14th and 19th centuries, in common with the rest of the Northern Hemisphere. Since ~1850, the LIA maximum, the climate has been warming and glaciers have been receding, albeit with brief periods of stabilization or even small advances (Zemp et al., 2015; Oliva et al., 2018). However, the nearly continuous shrinkage and wastage has accelerated in recent decades (Vidaller et al., 2021), similar to what is observed in the majority of mountain ranges in the world (Huss and 40 Hock, 2018; Hugonnet et al., 2021). The rapid shrinkage and wastage are mainly due to a warming of more than 1.2°C between 1949 and 2010 (Cuadrat et al., 2018), which could be even higher in high-elevation areas, affecting snow accumulation and its duration above ground (López-Moreno et al., 2019; López-Moreno, 2005). Due to the small size of Pyrenean glaciers, their evolution has been strongly influenced by the topographic characteristics of the surrounding area (size and height of cirques, aspect, slope, snow avalanche corridors, etc.): as well as an interannual climatic control, they now also have a topoclimatic 45 control (López-Moreno et al., 2006; Vidaller et al., 2021).

Consequently, the glacier area loss in the Pyrenees is remarkable: there were 52 glaciers in 1850, 39 in 1984, and 21 in 2020, corresponding to an area of 2,060 ha in 1850, 810 ha in 1984, and 232 ha in 2020, representing a loss of 88.8% of the glaciated area (Arenillas-Parra et al., 2008; Rico et al., 2017; Vidaller et al., 2021). In terms of ice thickness wastage, unlike area 50 shrinkage, there is in general a lack of information. Recent studies identified an ice thickness loss of 6.3 m for the period 2011–2020 as the mean for all the glaciers in the Pyrenean massif (Vidaller et al., 2021). Specifically, at Monte Perdido Glacier, López-Moreno et al. (2019) reported wastage of 6.1 m for the period 2011–2017. In the case of Ossoue Glacier, the geodetic mass balance was  $-31.3 \pm 1.9$  m w.e. (water equivalent) for the period 1983–2013 and  $-17.3 \pm 2.9$  m w.e. for the period 2001–2013 (Marti et al., 2015).

The Aneto Glacier is one of the southernmost glaciers in Europe (Grunewald and Scheithauer, 2010), and is the largest in the 55 Pyrenees although it is considered a very small glacier ( $<0.5$  km<sup>2</sup>) (Huss and Fischer, 2016). It is one of the most iconic of Pyrenean glaciers, as it is located below the highest peak of the mountain range (Aneto peak, 3,404 metres above sea level (m a.s.l.)) and it forms part of the natural and cultural landscape of the Posets-Maladeta Natural Park, attracting mountaineers and tourist to this Park (Carvache-Franco et al., 2022; Carrascosa-López et al., 2021). Additionally, this glacier is part of the Natural Monument of the Pyrenean Glaciers (Lampre-Vitaller, 2003), having an additional protection figure for this natural landscape 60 heritage. Unlike other alpine glaciers that are important water source in other mountain areas (Fountain and Tangborn, 1985; Braithwaite and Raper, 2002; Meier et al., 2007; Huss et al., 2017; Drenkhan et al., 2022) the Aneto glacier, as all Pyrenean glaciers, has a minor (and nearly negligible) contribution to rivers discharge in this region (López-Moreno et al., 2020). However, the ice shrinkage of Pyrenean glaciers has a clear impact on local erosion rates (Riihimaki et al., 2005), nutrient



fluxes, biochemistry and macroinvertebrate communities (Snook and Milner, 2001; Brown et al., 2007) or the microbiology  
65 of these emblematic landscapes and in surrounding downstream areas. The knowledge gap of these processes in the  
southernmost glaciers of Europe encourages and justifies the comprehension of their recent evolution. This study aims to  
exploit the largest spatio-temporal dataset of glacier observations to analyse the current state of the highest and largest glacier  
of the Pyrenees, the Aneto Glacier, combining state of the art methodologies. The evidence of Pyrenean glaciers demise in the  
next decades, thoroughly exemplified by this glacier (Vidaller et al., 2021) have a twofold interest; anticipate the evolution  
70 which might be expected in other temperate mountain glaciers and also to show the fast consequences of Climate Change in  
mountain areas to the society.

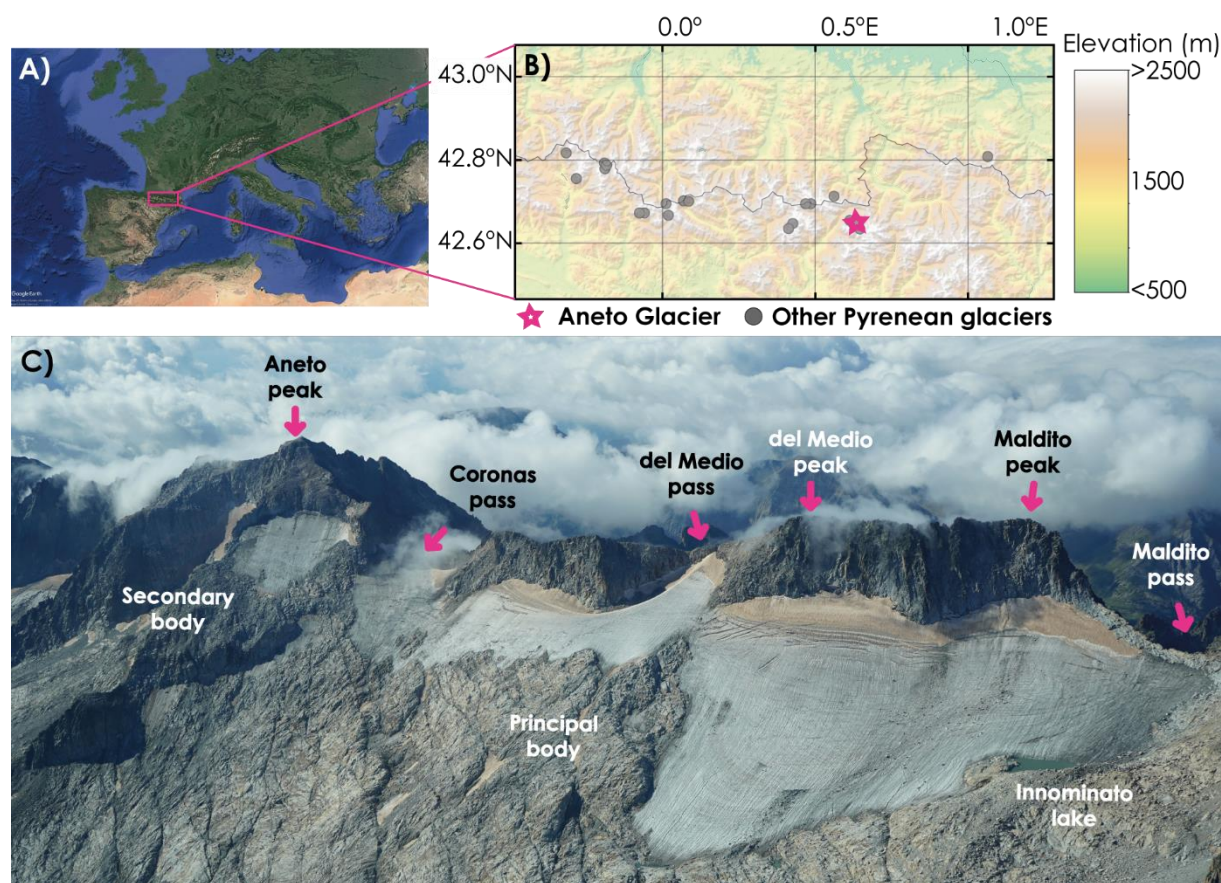
Despite the Aneto Glacier has not been subject to systematic annual mass balance monitoring to date, two recent studies  
(Campos et al., 2021; Vidaller et al. 2021) have analysed ice thickness variations for different time periods. Campos et al.,  
'Modeling the Retreat of the Aneto Glacier (Spanish Pyrenees) since the Little Ice Age, and Its Accelerated Shrinkage over  
75 Recent Decades'. presented a reconstruction of the area, volume, ice thickness, and Equilibrium Line Altitude (ELA) of Aneto  
Glacier for different time periods from the LIA to 2017, using photo interpretations and satellite imagery to calculate changes  
in glacier area and volume. Ice wastage in that work was derived from a steady-state model assuming a plastic ice rheology,  
combined with some Ground Penetrating Radar (GPR) profiles from 2008 (Campos et al., 2021). On the other hand, Vidaller  
et al. (2021) determined changes in glacier area and thickness for the period 2011–2020 with high spatial resolution in the 24  
80 Pyrenean glaciers (including Aneto Glacier). Shrinkage was determined based on satellite data and drone imagery, and the ice  
wastage was calculated by comparing 2011 and 2020 Digital Elevation Models (DEMs) (from Laser Imaging Detection and  
Ranging (LiDAR) and unmanned aerial vehicle (UAV), respectively). The results of this work for Aneto Glacier reported a  
shrinkage of 24.9% (69.3 ha in 2011 and 50.0 ha in 2020) and an average ice thickness decrease of 8.5 m.

In this study, we report the shrinkage and wastage of Aneto Glacier from 1981 to 2022 to build on the study of Vidaller et al.  
85 (2021) and try to determine the inflexion point at which the glacier shrinkage and wastage began its acceleration. We use high-  
resolution 3D point clouds from 1981 (from Structure-from-Motion (SfM) methods exploiting historical aerial photographs),  
2011 (from Spanish National Geographic Institute (IGN) LiDAR survey), 2020, 2021, and 2022 (from SfM methods using  
UAV flights). In addition, ice thickness was estimated from an intensive GPR survey conducted in July 2020. The combination  
of the three techniques allows accurate reconstruction of the glacier ice thickness in 1981 and its evolution until today.  
90 Moreover, the current ice volume and basal topography of the glacier could be determined. This information is critical for  
predicting the next changes in the glacier, since sectors can be delineated using most grid-like techniques, and the basal  
topography reveals sectors of likely lake formation after the ice disappears. The combination of these techniques provides an  
increase in knowledge over previous work because (1) we present data with high accuracy and lower uncertainty compared to  
previous studies and (2) we determine the evolution of Aneto Glacier for the longest period ever observed, by quantifying  
95 current ice thickness and basal topography, as well as the annual decrease in ice thickness from 1981 to 2022.



## 1.1 Study area

The Aneto Glacier is the largest glacier in the Pyrenees (47.9 ha in 2022), a mountain range where only four glaciers are larger than 10 ha. It is located in the Maladeta massif (Figure 1), on the northeast (NE) side, between the Maldito (3,354 m a.s.l.) and Aneto (3,404 m a.s.l.) peaks. The high elevation of this massif, with more than 40 peaks above 3,000 m a.s.l., has allowed the preservation of other smaller glaciers in the area (Eastern Maladeta and Tempestades) and ice patches (Western Maladeta, Coronas and Barrancs). In 2022, the Aneto Glacier consists of two bodies whose glacier front is at 3,026 m a.s.l. in the case of the main body and at 3,170 m a.s.l. in the case of the secondary body.



105 **Figure 1:** Location of the Aneto Glacier. (A) Map of Europe, with the pink rectangle delimiting the central part of the Pyrenees. © Google  
Maps (B) Topographic map of the central Pyrenees; the glaciers in this area are marked with grey dots and the location of the Aneto Glacier  
is marked with a pink star. (C) An aerial photo of Aneto Glacier in summer 2021. The main reliefs surrounding the glacier are indicated.

In this area, the 0°C isotherm ranges from 2,700 to 3,000 m a.s.l. (Jomelli et al., 2020), and the mean annual precipitation is about 2,000 mm, with winter and spring being the wettest seasons (Buisan et al., 2015). There are two weather stations in this  
110 area. One is located at Renclusa hut (2,140 m a.s.l.), where the maximum and minimum mean annual temperatures are 7 °C and 0.5°C, respectively, the maximum annual snow depth averages 4 m, and annual precipitation exceeds 1,300 mm (data from the AEMET database). The other station is located closer to Aneto summit, at 3,008 m a.s.l. since 2018 (data from the



115 Aragon Government and the Natural monument of Pyrenean Glaciers database); the mean annual temperature there was  $-1.4^{\circ}\text{C}$   
(maximum of  $15.4^{\circ}\text{C}$  and minimum of  $-21.0^{\circ}\text{C}$ ) and the maximum snow thickness was 2.8 m (the station is in a windy location,  
so snow accumulation is often limited by wind redistribution).

## 2 Data and methods

### 2.1 Imagery processing and DEM generation

#### 120 2.1.1 Historical aerial imagery

The earliest imagery dataset exploited here (1981 DEM) dates from September 1981. Aerial images were acquired by the Spanish National Geographic Institute (IGN) using analogue photogrammetric cameras (IGN, last accessed August 2022: <http://centrodedescargas.cnig.es/CentroDescargas/index.jsp>) aboard aircraft for national mapping surveys. The objective was to collect aerial photographs suitable to produce topographic maps of Spain at a scale of 1:50,000 and with contour intervals  
125 of 20 m (named MTN50). The overlap was 60% front and 30% side. The camera, *Wild lens cone RC 10*, had a sensor of  $230\times 230$  mm, a lens of 15 UAG II and a focal length of 152.12 mm; thus, an average image scale of 1:30,000 was obtained, with a Ground Sampling Distance (GSD) between 0.35 and 0.18 m/pixel. For this study, the historical aerial imagery was digitalized at a resolution of 15 microns. A total of 18 aerial images of the Aneto massif were used, taken from the same flight in late summer 1981.

130 Historical survey imagery was processed using Structure-from-Motion (SfM) (Snavely et al., 2006) with Agisoft Metashape Professional v1.6.3 software (<https://www.agisoft.com/>), which has shown reliable results when used for processing historical images (Llena et al., 2018). Processing parameters were set according to official Agisoft guidelines (denser point clouds, Bundle Block Adjustment (BBA), internal and external camera parameter calibration; Agisoft Metashape version 1.5, 2019). The SfM routines enabled generation of a dense point cloud ( $2.4\text{ pts/m}^3$ ), from which an orthomosaic with a resolution of 0.41  
135 m (used to calculate the glacier area) and a geoid-corrected Digital Terrain Model (DTM) with a grid cell size of 1.58 m were derived.

The historical survey imagery processing included the following workflow: (1) alignment of each flight line's cameras (3 lines total); (2) assignment of Ground Control Points (GCPs) based on clearly visible features such as individual large boulders and trail crossings or mountain summits; (3) derivation of accurate geographic coordinates and elevation information of these later  
140 GCPs using high-resolution satellite imagery (DigitalGlobe/GeoEye-1 imagery with 1 m resolution available through the QGIS



service ‘QuickMapServices’) and a 2020 UAV flight as a reference DTM (Vidaller et al., 2021); (4) taking advantage of GCPs, camera positions were realigned and all images were merged in one chunk using Agisoft Metashape Professional.

### 2.1.2 LiDAR survey

145 The 2011 high-resolution Digital Elevation Model (DEM) was derived from airborne LiDAR. The data were acquired in a flight of 9 November 2011, by the IGN (last accessed May 2022: <http://centrodedescargas.cnig.es/CentroDescargas/index.jsp>). The LiDAR device was a Leica ALS60 with a diode-pumped transmitter and a low-inertia/high-speed scanning mirror with a large aperture operating at a wavelength of 1,064 nm. The final georeferenced point cloud had an average density of 0.35 pts/m<sup>3</sup>. This information was processed and accurately geolocated by the IGN, which provides free access to the final 3D point cloud.

### 150 2.1.3 Unmanned Aerial Vehicle (UAV) imagery

The 2020, 2021, and 2022 glacier surface DEMs were obtained using a fixed-wing UAV (SenseFly eBee-X) on 12 September 2020, 1 October 2021, and 10 September 2022, respectively. The UAV was equipped with a SenseFly 3D S.O.D.A. digital camera (20Mp resolution) and GPS receivers enabling PPK (Post-Processed Kinematic) positioning systems (positioning accuracy <0.05 m after post-processing). As in previous studies (e.g. Vidaller et al., 2021), the UAV images had an overlap of 155 70% front and 50% side (note that the 3D S.O.D.A. camera obtains images with a tilt of 30°) with a final ground sampling distance (GSD) of 2.8 cm/px. The UAV images were processed using Pix4Dmapper (Pix4D) SfM software, in which the calculation of BBA and internal and external camera parameters calibration was enabled (more details on data processing in Vidaller et al. (2021)). Although Agisoft metashape could be used for this SfM processing, we preferred to use the same protocol described in previous works with UAV at this site to reduce uncertainties. Nonetheless comparison of point clouds 160 from both SfM software (Pix4Dmapper and Agisoft metashape) shows equivalent accuracies for working in highly heterogeneous areas (Mölg and Bolch, 2017; Llana et al., 2020). Due to the three UAV acquisitions having the same acquisition protocol, and the GPS-PPK geolocation (images geolocation with deviations below 4 cm), the comparison of these three point clouds yielded negligible deviations.

### 2.2 In situ Ground Penetrating Radar (GPR), processing and data interpolation

165 GPR uses the transmission and rebound of electromagnetic pulses at different frequencies to determine ice thickness and glacier interfaces (rocks, bedrock basin, snow, etc.) (del Rio et al., 2014). Different works have studied the variation in ice thickness, surface area or volume on glaciers using different techniques, which highlight the importance of the methodology to be applied in each case, considering its scope and limitations (Procházková, 2019; Bohleber et al., 2017; Marcer et al., 2017; Fischer, 2009).



170 GPR fieldwork was conducted on 25–26 July 2020, using a Malå Geoscience radar system consisting of a ProEx control unit  
and a 100-MHz Rough Terrain Antenna (RTA). Occasionally several transects were also carried out with the 100 MHz shielded  
antenna (see *Supplementary Material*). Georeferenced radargrams were created using the Atlas Link GNSS smart GPS antenna  
connected to the GPR, which were obtained in “time” tuning. A total of 32 georeferenced radargrams were recorded in the  
main glacier body in a common offset mode, corresponding to a length of 6.8 km and covering almost the entire glacier surface  
175 (more detailed information in *Supplementary Material, Figure S1*). The campaign was conducted during a period when the  
glacier surface was covered with snow, in order to allow safe displacement of the instrument and operators, thus hampering  
the observation of deeper ice layers. This required differentiation of the snow layer in post-processing to accurately quantify  
glacier thickness.

Radargrams were processed using ReflexW version 9.1.3 (Sandmeier Scientific Software), with the following workflow: (1)  
180 adjustment of the time origin ( $t=0$ ) to coincide with the arrival of the first surface signal on the glacier. (2) Homogenization of  
the trace increment, since the acquisition of the radargrams with the RTA antenna was done in time mode and varied in each  
radargram depending on the speed of movement of the antenna on the ground (0.1 m/ns was fixed since this was the smallest  
value obtained in the radargrams). (3) Background removal. (4) Correction of the energy loss of the signal when penetrating  
the terrain by applying a gain factor of 0.2 (energy decay). (5) Application of a frequency bandpass filter so that only signals  
185 with frequencies between 50 and 200 MHz remain (the nominal frequency of the antenna is 100 MHz).

As a first approximation, 0.17 m/ns was set as the propagation velocity of the waves in the glacier to get a first idea of the  
thickness of the snow and ice layers in the radargram representation. Snow and ice layers must be defined from the radargrams  
to create a thickness model of both. To do this, the wave propagation velocities (RWV) in both media must be available  
beforehand. In a similar study on Monte Perdido Glacier, RWVs of  $0.200 \pm 0.005$  m/ns for snow and  $0.163 \pm 0.007$  m/ns for  
190 ice were obtained for the 500 MHz and 200 MHz antennas, respectively (López Moreno et al., 2019). The coherence of these  
velocities was checked in the 1054 radargram at the points where diffraction hyperbolas occur (plot of diffraction hyperbolas  
in *Supplementary Material, Fig S2*).

The distribution of the GPR data does not follow a homogeneous pattern; the GPR record tracks were distributed along parallel  
and perpendicular lines forming an irregular grid (*Fig S1 in Supplementary Material*). Therefore, to determine the thickness  
195 of the glacier over its entire extent, an interpolation method is required. For this type of data, the interpolation method used  
was the Radial Basis Function (RBF) as Otero-García (2008) recommended. Given the poor distribution of the data, after  
several tests, the best method is to work with 16 neighbours, two per octant (the closest points in each direction), in a circular  
area with a radius of 457.62 m to find, in the same way, again, as Otero-García (2008). The thickness for glacier limits in 2020  
was established as zero m. To validate this interpolation method, the data were divided into two groups: Training with 70% of  
200 the sample and Test with the other 30%.



### 2.3 Glacier area outline, point cloud geolocation and glacier thickness change computation

The delineation of the Aneto Glacier area was done manually in a GIS software (ArcGIS), considering: (1) the orthomosaic of the historical aerial imagery from 1981; (2) a RapidEye satellite image from 2011 and improved outlines from RGI (RGI Consortium, 2017); and (3) the orthomosaics derived from UAV flights in 2020, 2021, and 2022. Due to the small extent of these very small glaciers, the calculation of glacier area considered slope to obtain the true glacier area (3D surface) rather than the 2D projection of glacier extent. This calculation is justified because glaciers are strongly bound to wall cirques and these have a strong slope; if this is not considered, the glacier area will be underestimated (Vidaller et al., 2021).

Data from DEM available for this work varied in accuracy. The most accurate geolocation is that of the UAV, which was used as a reference for the point cloud due to the PPK (Post Processed Kinematic) GPS geolocation technique (geolocation RMSE <math><0.05\text{ m}</math>). This geolocation error is equivalent for the 2020, 2021, and 2022 point clouds because the same acquisition protocol was used. To coregister the LiDAR point cloud (2011) and the point cloud from the historical aerial imagery (1981), several areas of stable terrain such as ridges, peaks, polished surfaces, etc. were selected in these later point clouds and in the 2020 UAV-derived point cloud. These areas were evenly distributed around the glacier. A rotation and translation matrix was calculated for these areas to align (separately) the 1981 and 2011 point clouds with that of 2020 using an ICP algorithm (Rajendra et al., 2014), from Cloud Compare software (Girardeau-Montaut, 2016). Subsequently, these matrices were applied to the entire point clouds to derive point clouds that were finally coregistered. Glacier surface changes between these dates were determined using the Cloud Compare tool M3C2 (James, 2017). Glacier change statistics were derived from this later comparison.

Glacier wastage was determined by considering only data within the smallest (or more recent) area of the glacier. When considering the oldest area, there are zones of the glacier that are not present in the most recent acquisitions, so the ice thickness change would be underestimated (Vidaller et al., 2021). The mass balance was calculated assuming a density conversion factor of  $850\text{ kg/m}^3$  (Huss, 2013).

With the aim of determining areas of future glacier lakes formation, the mountain basal topography was derived from the GPR interpolation and the 2020 UAV acquisition (subtraction of the 2020 glacier surface from the ice thickness interpolation from the GPR). From this basal topography the Topographic Position Index (TPI; de Reu et al., 2013) for 70, 100, 150 and 200 m search distances was derived to describe depression areas potentially favouring future lake areas.

### 2.4 Correction and accuracy assessment

GPR ice thickness measurements with a 100-MHz RTA antenna are subject to intrinsic error. Assuming a RWV velocity for ice of  $0.163\text{ m/ns}$ , the  $\lambda$ -value is  $1.63\text{ m}$ , so the minimum spatial resolution is  $\lambda/2 = 0.815\text{ m}$ . Summing this uncertainty for snow and ice gives a thickness resolution of  $1\text{ m}$  for this delineation. Thus, the uncertainty in the determination of the ice layer thickness is  $1.8\text{ m}$ .





To check the coherence of the determined thicknesses, a test was performed at all intersections between transects to detect any inconsistencies in the values. At these 28 intersections, the average difference is  $1.6 \pm 1.6$  ( $\sigma$ ) m, with some outliers of 3–5 m. This value is consistent with the uncertainty associated with RWV velocity and ice layers' delineation (1.8 m). The lengths of the radargrams were determined using ReflexW from the GPS coordinates coupled to the GPR (see *Supplementary Material* for more details).

To validate the interpolation of glacier thicknesses, 30% of the GPR data were randomly selected and the remaining 70% of the GPR dataset was used for the interpolation (Otero García, 2008). The mean error between the interpolated thickness and the thickness observed with the GPR was 0.0018 m, and the RMSE was 0.3021 m.

The delineation of glacier boundaries also has some uncertainty due to pixel size, geometric correction, visual identification, and the presence of residual snow or debris cover at the glacier boundaries. This surface uncertainty is 0.048 ha ( $48 \times 10^{-4}$  km<sup>2</sup>) for Aneto Glacier (Vidaller et al., 2021).

The coregistration of point clouds from historical aerial imagery and LiDAR survey with UAV surveys was tested in a buffer zone around the glacier, always using snow- and ice-free zones in both years of comparison. This means that the comparison of the 1981 and 2020 point clouds was performed in a buffer zone with a 300% larger extent around the 1981 glacier boundaries (over stable terrain); the coregistration error between the 2011 and 2020 point clouds was determined in the same way. In the first case for Aneto Glacier the RMSE is 0.06 m, in the second case 0.4 m (Vidaller et al., 2021).

### 3 Results

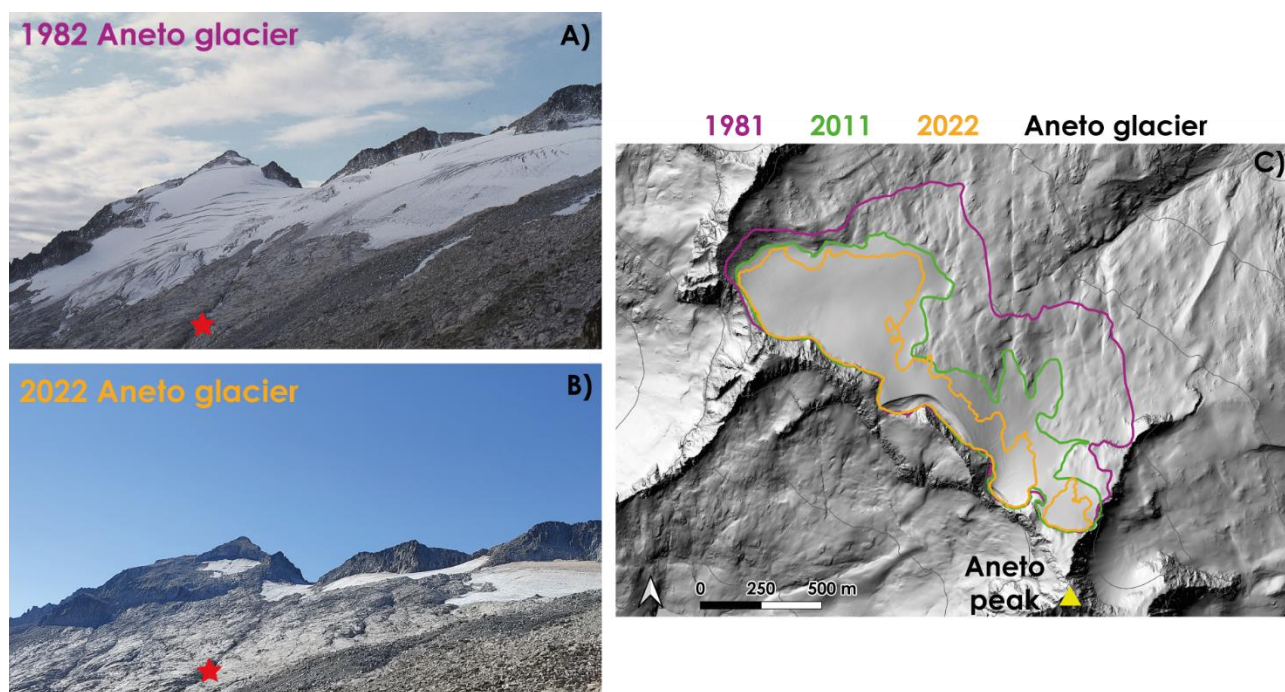
The extent of the Aneto Glacier has decreased significantly in the last few decades, from 135.7 ha in 1981 to 47.9 ha in 2022, i.e. by –64.7%. The shrinkage and wastage of the glacier continues, resulting in changes in area and the division of the glacier into two bodies. It is remarkable that the secondary body has no movement today (Table 1).

**Table 1:** Main characteristics of the Aneto Glacier over the years of the study.

Year	Area (ha)	Glacier front (m a.s.l.)	Area changes since 1981 (%)	Area changes since 1981 (% yr <sup>-1</sup> )
1981	135.7	2,828	–	–
2011	69.3	2,939	–49.0	–1.6
2020	Principal	47.8	–61.7	–1.6
	Secondary	4.2		
2021	Principal	46.1	–63.1	–1.6
	Secondary	3.9		
2022	Principal	45.1	–64.7	–1.6
	Secondary	2.8		



In 1981, the area of Aneto Glacier was 135.7 ha; in 2011, the area shrank to 69.3 ha, a loss of 49.0%. Between 2015 and 2016, the Aneto Glacier divided into two bodies; in 2020 the main body was 47.8 ha and the secondary body was 4.2 ha, a total of 52.0 ha. Table 1 results show that in the last 40 years the losses were 63.1% of its area ( $-1.6\% \text{ yr}^{-1}$ ). In 2022, the area has shrunk to 47.9 ha (45.1 ha for the main body and 2.8 ha for the secondary body), a decrease of 64.7% compared to 1981 (Figure 2). This decrease represents a retreat of the lowest glacier front from 2,828 m a.s.l. in 1981 to 2,939 m a.s.l. in 2011, 3,011 m a.s.l. in 2020, 3,014 m a.s.l. in 2021, and 3,026 m a.s.l. in 2022.



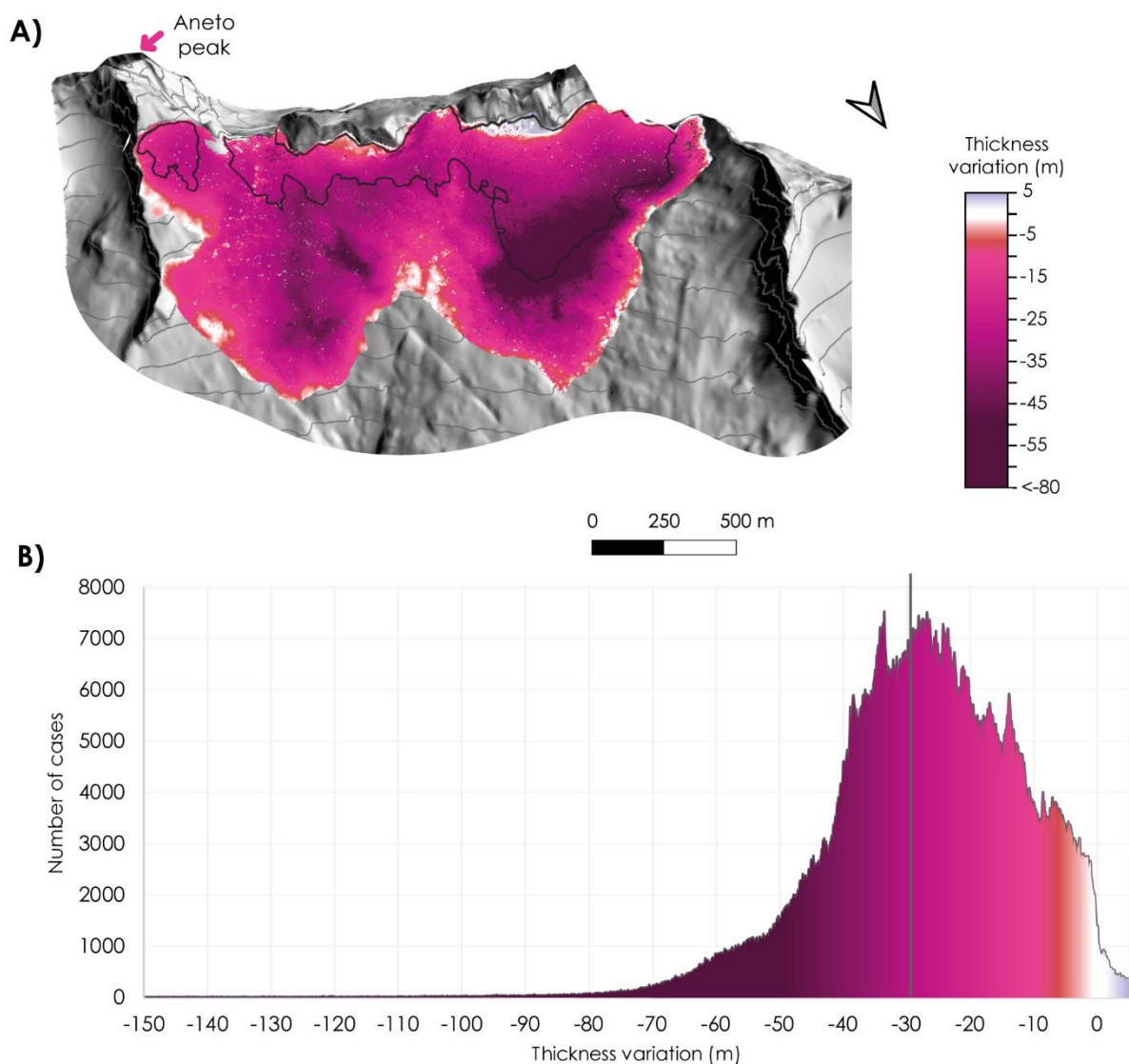
260 **Figure 2:** Appearance of the Aneto Glacier during the study period. (A) Photo (Fernando Biarge, Fototeca DPH) corresponding to Aneto  
Glacier in 1982. (B) Photo corresponding to Aneto Glacier in 2022. The red stars refer to the same location in both photos. (C) Map showing  
differences in the area of the glacier during the study period; the purple line delineates the extent of the glacier in 1981, the green line in  
2011, and the orange line in 2020. The shading of the terrain was calculated from the 2011 LiDAR. The yellow triangle represents the  
summit of Aneto peak.

265 A comparison of the 1981 and 2022 point clouds shows a mean ice thickness loss of 30.51 m (Figure 3) in this period and  
considering only the area occupied by the glacier in 2022 (considering the 1981 glacier extent, the ice thickness loss is 24.1  
m). This means that the glacier lost on average  $0.6 \text{ m yr}^{-1}$  over the entire glacier and  $0.7 \text{ m yr}^{-1}$  in the currently glaciated area  
during the 1981–2022 period. The thickness losses are not evenly distributed. The highest ice thickness variations are in the  
middle of the main body, while the lowest variations are in the secondary body (Figure 3A). More than 41% of the 2022 glacier  
270 area has lost more than the mean (30.5 m) (Figure 3B).

The results indicate an acceleration in glacier wastage in the last decade. The mean ice thickness loss for the period 1981–  
2011 is 17.8 m ( $0.6 \text{ m yr}^{-1}$ ) and 12.6 m ( $1.1 \text{ m yr}^{-1}$ ) for the period 2011–2022, representing an increase of ice wastage in the



later period of 200% compared to 1981–2011. The available information for the 2020–2021 and 2021–2022 annual comparisons highlights the high interannual variability of ice loss, with mean ice thickness decreases of 1.5 m and 3.2 m, respectively. As for the specific mass balance, the losses are 0.6 m w.e. yr<sup>-1</sup> for the period 1981–2022, 0.5 m w.e. yr<sup>-1</sup> for the period 1981–2011, 1.0 m w.e. yr<sup>-1</sup> for the period 2011–2022, 1.2 m w.e. yr<sup>-1</sup> for the period 2020–2021, and 2.7 m w.e. yr<sup>-1</sup> for the period 2021–2022.



280 **Figure 3:** (A) Thickness change of Aneto Glacier from 1981 to 2022. In the upper map, the black line delineates the glacier in 2020. The arrow indicates the north direction. (B) Frequency distribution (number of cases) of thickness changes. The vertical black line defines the mean value of the ice thickness decrease.



The GPR survey of the main body of the glacier in 2020 reveals a mean glacier thickness of 15.0 m, with a maximum glacier thickness of 44.7 m (Figure 4A). This maximum glacier thickness was measured in the western part of the glacier, near the  
285 Maldito (3,354 m a.s.l.) and Del Medio (3,349 m a.s.l.) peaks. The greatest thickness was measured in the upper parts of the glaciers in the elevation range between 3,200 and 3,350 m a.s.l. (Figure 4A and 4B). In some elevation ranges (between 3,100 m and 3,180 m a.s.l.), the glacier thickness is lower than expected, considering the trend of increase with increasing elevation. This is mainly due to the presence of a relatively thick sector (up to 39 m) between 3,000 and 3,100 m in the western part of the glacier, which affects the mean values observed in this elevation range. Figure 4A also shows the presence of very narrow  
290 and shallow ice sectors (light blue areas) adjacent to the cirque wall in two places, indicating an imminent separation of the glacier into three ice bodies.

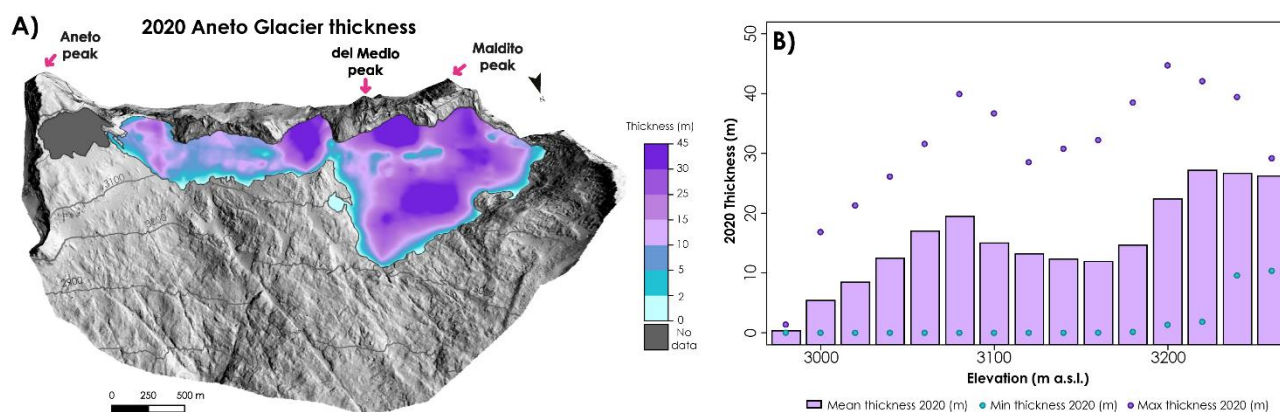
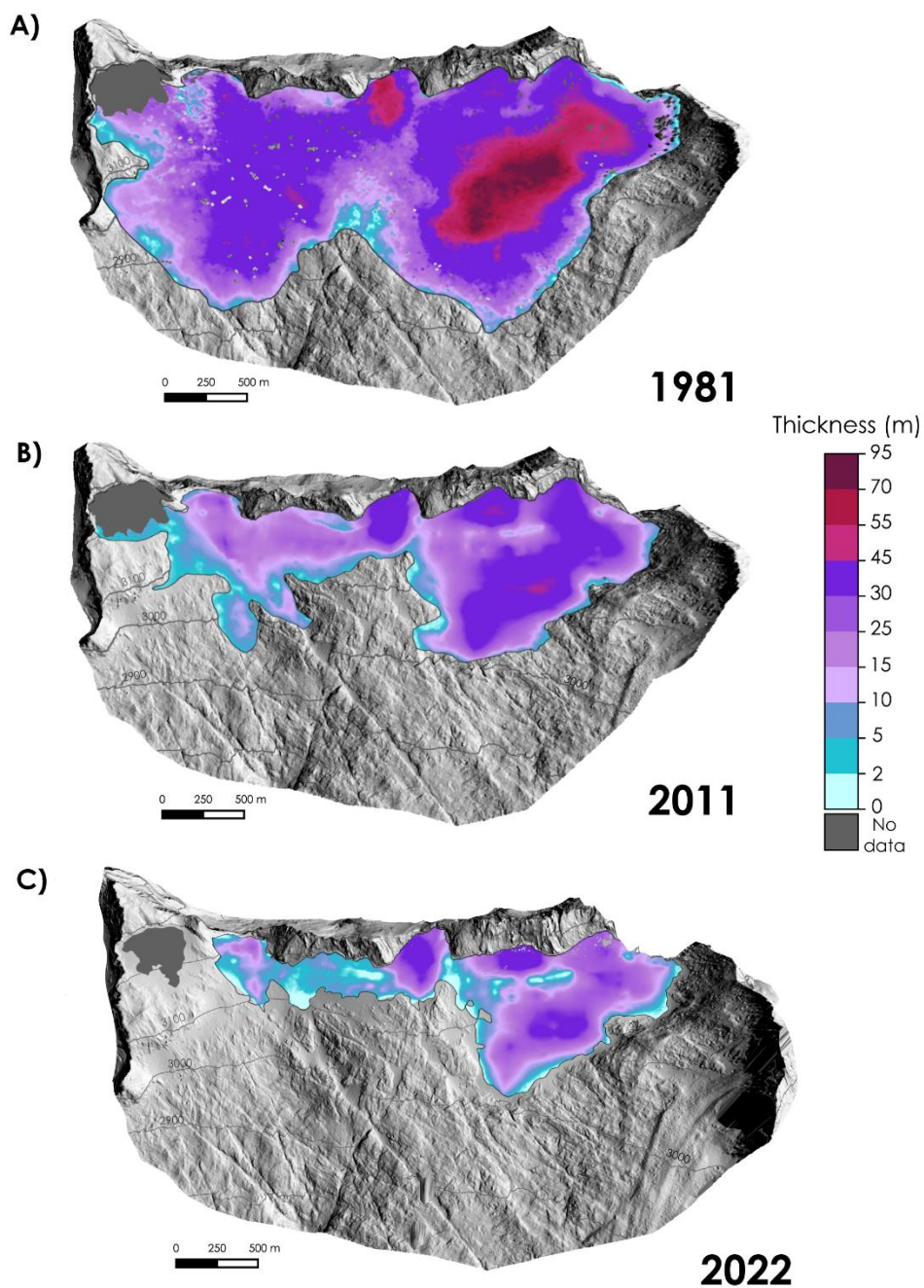


**Figure 4:** Ice thickness of Aneto Glacier in 2020. In map (A), the blue colour represents the zones of lesser ice thickness that are about to disappear, in contrast to the purple colours that represent the greatest ice thickness. The secondary body of the Aneto Glacier is coloured grey because no data are available for this glacier body and therefore no interpolation is possible. The diagram (B) shows the glacier thickness in 2020 as a function of the 20 m elevation levels. The bars describe the mean thickness, the blue dots the minimum thickness, and the purple dots the maximum thickness of the individual elevation levels.

By combining information on glacier thickness derived from the 2020 GPR observation with thickness losses estimated (with UAV and historical images) for 2011–2020 and 1981–2020, as well as those observed in subsequent periods (2020–2022) with  
300 UAV, ice thicknesses for 1981, 2011 and 2022 were reconstructed (Figure 5). In 1981 (Figure 5A), the pattern of ice thickness distribution shows some differences compared to recent periods. In 1981, the maximum glacier thickness was found in the middle elevations of the western part, where ice thickness reached 90 m. Below del Medio pass, the glacier thickness was also very high, almost 70 m. In 1981, the maximum thickness was 96.5 m, and the mean thickness of the glacier was 32.9 m. In 2011 (Figure 5B), the distribution pattern of ice thickness on Aneto Glacier is very similar to that of 2020 (Figure 4A);  
305 maximum ice thickness was measured below the Maldito peak and in the lower western part of the glacier. The maximum ice thickness at that time was 52.5 m, while the mean thickness of the glacier was 19.2 m. In 2022 (Figure 5C), the ice thickness distribution has not changed markedly, and the greatest thickness continues to be under the Maldito pass and peak, and in the middle of the main body of Aneto Glacier. In this latter year, the average ice thickness is 11.9 m, and the maximum ice



thickness is 44.0 m, but although the maximum ice thickness exceeds 44 m, 43.0% of Aneto Glacier in 2022 has an ice  
310 thickness of less than 10 m.





315 **Figure 5:** Reconstruction of the ice thickness of Aneto Glacier at different times during the study period. (A) shows the thickness in 1981, (B) shows the thickness in 2011, and (C) shows the thickness in 2022. The blue colour represents the zones of lower ice thickness that are about to disappear, in contrast to the red colours that represent the greatest ice thickness. The secondary body of the Aneto Glacier is coloured grey because no data are available for this glacier body and therefore no interpolation is possible.

As is well known, glaciers erode the surface beneath the ice mass so that the subglacial topography is not a flat surface. Glacial erosion creates thresholds and depressions, which in some cases are filled by meltwater from the glacier, forming glacial lakes (Shugar et al., 2020; Yao et al., 2018). This is the case with Ibón Innominato, a new small proglacial lake formed in 2015 as a result of the retreat of the Aneto Glacier. Today, it is the highest mountain lake in the Pyrenees (3,150 m a.s.l.). Due to the continuous shrinkage of the glacier, this lake grows simultaneously with the retreat of the Aneto Glacier, although it is ice-free only 3–4 months a year (July–October). In 2020, its area was 0.4 ha and in 2022 it was 0.5 ha, an increase in area of 26.5% for the period 2020–2022, mainly due to the frontal retreat of the Aneto Glacier by about 15.2 m.

320 Depression areas of the subglacial topography have been analysed through the TPI computed for four search distances (75–100–150–200 m). This index has already been used in studies of debris-covered glaciers (Westoby et al., 2020). to determine areas with potential accumulation of rocks, but as far as the authors know, this is the first time this index has been exploited to determine areas of potential lake formation after mountain glaciers retreat. The TPI spatial distribution depicts depression areas that could fill with water after the ice disappears (blue colours in Figure 6). For example, under the del Medio peak and “Medio” pass, a remarkable depression for 150 and 200 m search distances is observed. These areas nowadays have the highest  
330 ice thicknesses, and thus lakes could be found in these areas when the glacier has completely disappeared.

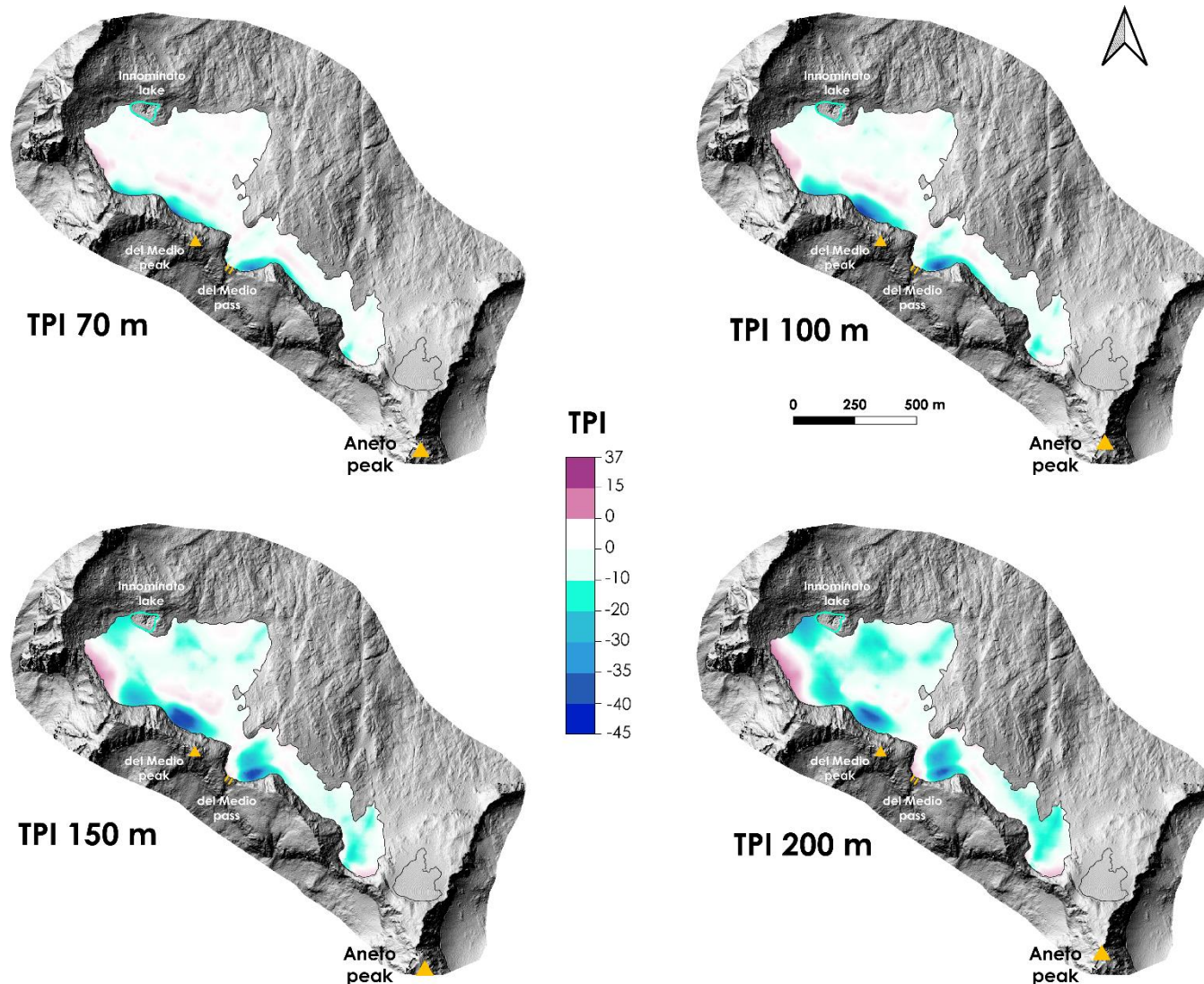


**Figure 6:** TPI 70, 100, 150 and 200 m based on the basal topography derived from the GPR data from 2020. Negative/positive values (blue/red colours) represent locations that are lower/higher than their surroundings.

#### 4 Discussion

##### 335 4.1 Recent changes of the Aneto glacier: a foretaste of the future evolution of European glaciers

Annual area loss decreased uniformly over time ( $-2.2 \text{ ha yr}^{-1}$ ,  $-2.2 \text{ ha yr}^{-1}$ ,  $-2.1 \text{ ha yr}^{-1}$ , and  $-2.1 \text{ ha yr}^{-1}$  from 1981 to 2011, 2020, 2021, and 2022, respectively). However, it must be noted that the relative changes are larger in the latter years, since the losses occurring in the most recent period are measured with respect to a progressively smaller area. Thus, there is not a recent acceleration of the shrinkage per year but the relative area loss has increased. Glacier thickness change rates have increased



340 during the study period ( $-0.6 \text{ m yr}^{-1}$ ,  $-0.6 \text{ m yr}^{-1}$ ,  $-0.7 \text{ m yr}^{-1}$ , and  $-0.7 \text{ m yr}^{-1}$  from 1981 to 2011, 2020, and 2022, respectively), indicating an acceleration of glacier volume wastage. In terms of specific mass balance, the losses are  $0.6 \text{ m w.e. yr}^{-1}$  for the period 1981–2022,  $0.5 \text{ m w.e. yr}^{-1}$  for the period 1981–2011,  $1 \text{ m w.e. yr}^{-1}$  for the period 2011–2022,  $1.2 \text{ m w.e. yr}^{-1}$  for the period 2020–2021, and  $2.7 \text{ m w.e. yr}^{-1}$  for the period 2021–2022. This wastage is mainly accelerated (among other factors) by the fact that the accumulation zone over the glacier in summer is negligible, especially during very hot summers; and the ablation zone covers the entire glacier, as no ELA is observed for some years. Unfortunately, due to the small extent of this glacier no reliable satellite observations of sufficient resolution are available for Aneto Glacier ELA in late summer, and this absence of accumulation area is based on field work observations of UAV operators.

Various studies of other glaciers in the Pyrenees have also shown a continuous increase in glacier thickness and area loss, with a high interannual variability but a clear negative trend over longer time periods. These works focused on Monte Perdido Glacier (López-Moreno et al., 2019), Ossoue Glacier (Gascoïn and René, 2018), Maladeta Glacier (Pastor Argüello, 2013) and La Paul Glacier (Rico et al., 2015). The mean annual specific mass balance values of  $-0.6 \text{ m w.e. yr}^{-1}$  on Aneto Glacier determined for the period 1981–2022 are similar to those in other studies in the Alps, such as Davaze et al. (2020), who estimated an annual mass balance of  $-0.7 \text{ m w.e. yr}^{-1}$  from 2000 to 2016 for 239 Alpine glaciers. Similarly, Carturan et al. (2016) determined the mean annual mass balance of nine Italian glaciers from 2004 to 2013, which ranged from  $-1.8$  to  $-0.8 \text{ m w.e. yr}^{-1}$ . This is also supported by other climatic data showing an increase in air temperatures over the past century (Bolch et al., 2012; Rabatel et al., 2013), particularly a sharp rise in temperatures at high elevations and low latitudes (Vuille et al., 2008; Pepin et al., 2015), accompanied by a shorter duration of seasonal snow cover (Brown and Mote, 2009).

Vidaller et al. (2021) describe the changes in ice thickness of the Aneto Glacier (among other glaciers of the Pyrenees) based on an ice thickness decrease of  $8.5 \text{ m}$  during the period 2011–2020. Based on the ice thickness reconstruction data of the Aneto Glacier presented in this study, the mean ice thickness in 2020 was  $15.0 \text{ m}$ , while in 2011 it was  $19.2 \text{ m}$ , so the loss is  $4.2 \text{ m}$ . This difference is due to the fact that the mean ice thickness of 2011 was calculated based on the extent of 2011 and the ice thickness of 2020 was calculated based on the area of 2020, while in the case of Vidaller et al. (2021) the wastage was calculated considering only the ice thickness losses within the glacier area of 2020. A similar problem exists when comparing the remaining ice thickness in 1981 ( $32.9 \text{ m}$ ) and in 2022 ( $11.9 \text{ m}$ ) with the ice thickness losses for the period 1981–2022 ( $30.5 \text{ m}$ ). Remaining ice thickness in 1981 is similar to those losses calculated for the period 1981–2022; meanwhile the remaining average ice thickness is  $11.9 \text{ m}$ . The mean ice thickness for a particular year was calculated based on the extent observed for that year.

#### 4.2 The importance of the methods

Remote sensing techniques have developed rapidly in recent years, allowing observation of the Earth's surface with a spatial resolution that was previously impossible. This work exploits historical aerial photographs to reconstruct a digital surface model for the year 1981 and provides a comparison to observe changes in landscapes and surfaces in detail.





Campos et al. (2021) calculated changes in Aneto Glacier from the LIA to 2017 using data from 1957, 1983, 2000, 2006, 2015, and 2017. In 1983, they reported an area of 103.2 ha, in contrast to the 135.7 ha for 1981 described in this work. The large difference may be due in part to the fact that they did not consider the slope angle of the terrain in their calculations (2D vs 3D surface). Nonetheless, considering our delineation, but ignoring the effect of slope angle on the area estimate, we would have reported a value of 115.5 ha for 1981, which underestimates our value by 20%. This study also uses the National Fly photograms to convert to point clouds, accounting for stable GCP during the study period. This is a more accurate method because it avoids distortion of the *Plan Nacional de Ortofotografía Aérea* (PNOA) orthophotos used by Campos et al. (2021), who acknowledge a source of uncertainty: “The extension for the 1983 stage should be considered with caution, due to the lower quality of the 1983 aerial image.” The area determined in our study is closer to that reported by Arenillas-Parra et al. (2008), who reported an extent of 136 ha for Aneto Glacier in 1982 based on aerial photographs of a specific flight in the glaciated areas of the Pyrenees.

The values of ice thickness from the GPR reported in Campos et al. (2021) also show significant differences not consistent with our results. In 1994, the ERHIN programme estimated a maximum ice thickness of 52 m using 17 transects spaced 100 m apart (Arenillas-Parra et al., 2008; Jiménez-Vaquero, 2016). In 2008, those authors determined a maximum ice thickness of 30 m calculated from 31 GPR transects (Jiménez-Vaquero, 2016). Considering these data, Campos et al. (2021) reconstructed the subglacial topography of Aneto Glacier and based on this topography they determined a maximum ice thickness of 55 m for 1983, 37 m for 2006, and 29 m for 2015. These values are in stark contrast to our estimates (maximum 96.5 m in 1981, 52.5 m in 2011, 44.7 m in 2020, 43.5 m in 2021, and 41.8 m in 2022). Comparing the values of remaining thickness reported in 2008 (maximum ice thickness of 30 m (Jiménez-Vaquero, 2016)) and the rate of wastage ( $-1.0 \text{ m yr}^{-1}$ ) established by Vidaller et al. (2021) for the period 2011–2020, the expected maximum thickness in 2020 would be 18 m instead of the 44.7 m we observed in 2020. Additionally, large areas currently covered by the glacier would be ice-free according to the previous wastage estimates. Considering that we used comparable values for wave propagation velocity of GPR signal to those used in the above-cited work, the differences between previous literature and the glacier thicknesses reported here are likely related to the more modern and accurate antennas used in our survey and the much denser net of transects conducted in the 2020 campaign. This methodology significantly reduces the uncertainties associated with the interpolation process, making the results obtained here more robust, and also permits a better understanding of the glacier’s dynamic and its future behaviour.

#### 4.3 Future perspectives

The rate of shrinkage and wastage calculated in this study and the reconstruction of ice thickness for the year 2022 indicate the critical situation of this glacier. There are no signs of slowdown in glacier shrinkage and wastage; on the contrary, we have observed the high vulnerability of the Aneto Glacier to the occurrence of extremely hot summers in recent years. Taking into account the average current glacier thickness of 11.9 m, we can affirm that the Aneto Glacier is indeed in its terminal stage, with evident fragmentation into smaller ice bodies, the absence of a significant accumulation zone and obvious signs of ice stagnation. In this context, glacier thinning and wastage is exposing new areas of unconsolidated bedrock material (granite



405 boulders and debris) and destabilizing cirque walls in many areas. This process is also accompanied by a degradation of surrounding wall permafrost (Rico et al., 2021). Under this situation the occurrence of unusual warm periods such as the observed in the 2021-2022 period, triggered hazardous rockfalls as were also noticed in other mountain areas (Huggel et al., 2010; Kellerer-Pirklbauer et al., 2012).

Another aspect that determines the evolution of the Aneto Glacier is the darkening of the glacier surface. Early spring/summer snowmelt and glacier wastage result in a grey/dark appearance of the glacier surface, decreasing the albedo effect and increasing the heat absorption, which leads to an acceleration of the shrinkage and wastage of the glacier Shaw et al., ‘Glacier Albedo Reduction and Drought Effects in the Extratropical Andes, 1986–2020’.. The obvious similarities with the remaining glaciers of the range suggest that the Pyrenees may become an ice-free mountain range in the next few decades.

415 The rise in temperature in recent decades, combined with a slight decrease in precipitation, has resulted in less snow accumulation during the winter months. This results in longer exposure of the glacier during the ablation season, which increases the melting of the glacier from year to year. Compared to Pyrenean glaciers that have a minimal contribution to water resources in downstream areas (López-Moreno et al., 2020; Milner et al., 2017), changes in snowpack can lead to severe changes in the downstream water regime (García-Ruiz et al., 2011).

Also of note is the presence and development of new proglacial lakes, as in the case of Ibón Innominato. This small lake is in constant change due to shrinkage and wastage of the glacier, where the retreat of the glacier front has opened new outlets beneath the glacier, and consequently the water level of the lake decreases. Similarly, as the Aneto Glacier shrinks, other lakes would be formed in the depression areas derived from the subglacial topography The presence of proglacial lakes negatively affects the glacier’s equilibrium by acting as an energy collector and accelerating the rate of thawing at the front of the glacier Otto, ‘Proglacial Lakes in High Mountain Environments’.. In addition, the dark appearance of the glacier surface caused a decrease in albedo and therefore an increase in the wastage and shrinkage of the glacier Yue et al., ‘Variation in Albedo and Its Relationship With Surface Dust at Urumqi Glacier No. 1 in Tien Shan, China ’..

425 On the other hand, the maximum ice thickness (>44 m) is located under Maldito pass, a protected area fed by avalanche channels and protected by the shadow of Maldito peak. In these areas, longer persistence of the ice body is expected.

The fast shrinkage of Aneto Glacier in the last decades and the relatively low ice thickness observed together with the potential development of new lakes, clearly show the consequences of climate change in mountain areas. Those changes happening nowadays in most mountain glaciers (Kääb et al., 2021; Barrand et al., 2017; DeBeer and Sharp, 2009) will have a major impact on mountain landscapes and ecosystems (Huss et al., 2017) showing the necessity of monitoring and understanding the recent fast evolution of these environments.



## 435 5 Conclusions

Aneto Glacier, although it is considered a very small glacier, is the largest glacier in the Pyrenees and also the largest in southern Europe. However, climate change has accelerated its disappearance, in common with other glaciers in the range. The evolution of close-range remote sensing techniques allowed us to observe the glacier surface in a very high level of detail that permits comparison between different years' surface (DEMs) of the glacier and evaluation of its changes.

440 For the period 1981–2022 the Aneto Glacier surface has diminished 64.7% (from 135.7 ha to 47.9 ha) and its front has shifted from 2,828 m to 3,026 m. It has also been divided into two bodies between 2015 and 2016 and a proglacial lake has appeared in front of it. The annual rate of area decrease has been constant over time ( $-2.2 \text{ ha yr}^{-1}$  and  $-2.1 \text{ ha yr}^{-1}$  from 1981 to 2022 and from 2021 to 2022, respectively), but the relative shrinkage of the glacier surface has increased during the study period.

The ice thickness wastage was estimated at 30.5 m on average for this 41-year period (with maximum losses over 80 m), with 445 a specific mass balance of  $0.6 \text{ m w.e. yr}^{-1}$ . However, the annual thickness loss ratio has been increasing, in fact quadrupled ( $2.7 \text{ m w.e. yr}^{-1}$  for the period 2021–2022) over the period 1981–2022. Using GPR measurements, we have estimated a mean of 44.7 m of ice thickness in 2020. GPR data and ice thickness losses estimated with UAV data have been used to infer the actual mean ice thickness, which is 11.9 m. The ice thickness distribution shows areas around the glaciers with very little thickness ( $<2 \text{ m}$ ), so these zones are very close to becoming deglaciated during the coming summers.

450 The shrinkage and wastage of Aneto Glacier indicate the critical situation of this ice mass. It is in its terminal stage, displaying fragmentation into smaller ice bodies and the presence of debris cover in some areas.

### Acknowledgments:

455 This work was supported by the Interreg-POCTEFA project OPCC ADAPYR and Spanish Ministry of Economy and Competitiveness project “CGL2017-82216-R” and the Spanish Ministry of Science and Innovation “PID2020-113247RB-C21 and PID2021-124220ob-100/MARGISNOW”. J. Revuelto has been supported by the IJC2018-036260-I (Juan de la Cierva I) and RYC2021-033859-I (Ramón y Cajal) projects. I. Vidaller is supported by the Grant FPU18/04978 and is studying the PhD programme in the University of Zaragoza. E. Izagirre is supported by the Grant PPGI19/02 (UPV/EHU) and the Consolidated 460 Research Group IT1678-22 (Basque Country Government). Esteban Alonso-González has been funded by the CNES postdoctoral fellowship.

### Contributions:

Conceptualization, I.V., J.I.L.M., E.I., J.R.; methodology, I.V., E.I., L.M.dR., J.R.; software, I.V., E.I., J.R; validation, I.V., 465 E.I., L.M.dR., J.R, J.I.L.M.; formal analysis, I.V., J.R., E.I., investigation, all authors.; resources, J.I.L.M.; data acquisition, all



authors; writing—original draft preparation, I.V.; writing—review and editing, all authors; visualization, I.V.; funding acquisition, J.I.L.M. All authors have read and agreed to the published version of the manuscript.

## 470 References

- Arenillas-Parra, M., Cobos-Campos, G., and Navarro-Caravallo, J.: Datos sobre la nieve y los glaciares en las cordilleras españolas. El programa ERHIN (1984–2008), Ministerio., Madrid, 236 pp., 2008.
- Barrand, N. E., Way, R. G., Bell, T., & Sharp, M. J. (2017). Recent changes in area and thickness of Torngat Mountain glaciers (northern Labrador, Canada). *The Cryosphere*, 11(1), 157–168. <https://doi.org/10.5194/tc-11-157-2017>
- 475 Bohleber, P., Sold, L., Hardy, D. R., Schwikowski, M., Klenk, P., Fischer, A., Sirguey, P., Cullen, N. J., Potocki, M., Hoffmann, H., and Mayewski, P.: Ground-penetrating radar reveals ice thickness and undisturbed englacial layers at Kilimanjaro’s Northern Ice Field, *Cryosph.*, 11, 469–482, <https://doi.org/10.5194/tc-11-469-2017>, 2017.
- Bolch, T., Kulkarni, A., Kääb, A., Huggel, C., Paul, F., Cogley, J. G., et al. (2012). The State and Fate of Himalayan Glaciers. *Science*, 336(6079), 310–314. <https://doi.org/10.1126/science.1215828>
- 480 Braithwaite, R. J. and Hughes, P. D.: Regional geography of glacier mass balance variability over seven decades 1946–2015, <https://www.frontiersin.org/article/10.3389/feart.2020.00302>, 2020.
- Braithwaite, R. J., & Raper, S. C. B. (2002). Glaciers and their contribution to sea level change. *Physics and Chemistry of the Earth, Parts A/B/C*, 27(32), 1445–1454. [https://doi.org/https://doi.org/10.1016/S1474-7065\(02\)00089-X](https://doi.org/https://doi.org/10.1016/S1474-7065(02)00089-X)
- 485 Brown, L. E. E. E., Hannah, D. M., & Milner, A. M. (2007). Vulnerability of alpine stream biodiversity to shrinking glaciers and snowpacks. *Global Change Biology*, 13(5), 958–966. <https://doi.org/https://doi.org/10.1111/j.1365-2486.2007.01341.x>
- Brown, R. D., & Mote, P. W. (2009). The Response of Northern Hemisphere Snow Cover to a Changing Climate. *Journal of Climate*, 22(8), 2124–2145. <https://doi.org/10.1175/2008JCLI2665.1>
- 490 Buisan, S. T., Saz, M. A., and López-Moreno, J. I.: Spatial and temporal variability of winter snow and precipitation days in the western and central Spanish Pyrenees, *Int. J. Climatol.*, 35, 259–274, <https://doi.org/https://doi.org/10.1002/joc.3978>, 2015.
- Campos, N., Alcalá-Reygosa, J., Watson, S. C., Kougkoulos, I., Quesada-Román, A., and Grima, N.: Modeling the retreat of the Aneto Glacier (Spanish Pyrenees) since the Little Ice Age, and its accelerated shrinkage over recent decades, 31, 495 1315–1326, <https://doi.org/10.1177/09596836211011678>, 2021.
- Carrascosa-López, C., Carvache-Franco, M., & Carvache-Franco, W. (2021). Perceived Value and Its Predictive Relationship with Satisfaction and Loyalty in Ecotourism: A Study in the Posets-Maladeta Natural Park in Spain.



- Sustainability*, 13(14). <https://doi.org/10.3390/su13147860>
- 500 Carturan, L., Baroni, C., Brunetti, M., Carton, A., Dalla Fontana, G., Salvatore, M. C., Zanoner, T., and Zuecco, G.: Analysis of the mass balance time series of glaciers in the Italian Alps, *Cryosphere*, 10, 695–712, <https://doi.org/10.5194/tc-10-695-2016>, 2016.
- Carvache-Franco, M., Carrascosa-López, C., & Carvache-Franco, W. (2022). Market Segmentation by Motivations in Ecotourism: Application in the Posets-Maladeta Natural Park, Spain. *Sustainability*, 14(9). <https://doi.org/10.3390/su14094892>
- 505 Cuadrat, J. M., Valero-Garcés, B., Moreno, A., Verfaillie, D., Galop, D., Rodríguez, E., Tejedor, E., Lostres, F. B., Soubeyroux, J.-M., Cunillera, J., García-Ruiz, J. M., López-Moreno, J. I., Trapero, L., Pons, M., Prohom, M., Saz, M. A., González-Sampériz, P., Ramos, P., Amblar, P., Copons, R., Serrano-Notivoli, R., Gascoin, S., and Luna, Y.: El cambio climático en los Pirineos: impactos, vulnerabilidades y adaptación, 149 pp., 2018.
- Davaze, L., Rabatel, A., Dufour, A., Hugonnet, R., and Arnaud, Y.: Region-wide annual glacier surface mass balance  
510 for the European Alps from 2000 to 2016, 2020.
- DeBeer, C. M., & Sharp, M. J. (2009). Topographic influences on recent changes of very small glaciers in the Monashee Mountains, British Columbia, Canada. *Journal of Glaciology*, 55(192), 691–700. <https://doi.org/10.3189/002214309789470851>
- Drenkhan, F., Buytaert, W., Mackay, J. D., Barrand, N. E., Hannah, D. M., & Huggel, C. (2022). Looking beyond  
515 glaciers to understand mountain water security. *Nature Sustainability*. <https://doi.org/10.1038/s41893-022-00996-4>
- Fischer, A.: Calculation of glacier volume from sparse ice-thickness data, applied to Schaufelferner, Austria, *J. Glaciol.*, 55, 453–460, <https://doi.org/10.3189/002214309788816740>, 2009.
- Fountain, A. G., & Tangborn, W. V. (1985). The Effect of Glaciers on Streamflow Variations. *Water Resources Research*, 21(4), 579–586. <https://doi.org/https://doi.org/10.1029/WR021i004p00579>
- 520 García-Ruiz, J. M., Palacios, D., Andrés, N., and López-Moreno, J. I.: Neoglaciation in the Spanish Pyrenees: a multiproxy challenge, *Mediterranean Geoscience Reviews*, 2, 21–36, 2020.
- García-Ruiz, J. M., López-Moreno, J. I., Vicente-Serrano, S. M., Lasanta-Martínez, T., & Beguería, S. (2011). Mediterranean water resources in a global change scenario. *Earth-Science Reviews*, 105(3), 121–139. <https://doi.org/https://doi.org/10.1016/j.earscirev.2011.01.006>
- 525 Gascoin, S. and René, P.: Recent evolution of the Vignemale glaciers (2013–2017), 2018.
- Girardeau-Montaut, D.: CloudCompare, Retrieved from CloudCompare <https://www.danielgm.net/cc>, 2016.
- Grove, J. M.: Little ice ages: Ancient and modern, Routledge., London, 1–718 pp., <https://doi.org/10.4324/9780203505205>, 2004.
- Grunewald, K. and Scheithauer, J.: Europe’s southernmost glaciers: response and adaptation to climate change, *Journal of Glaciology*, 56, 129–142, [https://doi.org/DOI: 10.3189/002214310791190947](https://doi.org/DOI:10.3189/002214310791190947), 2010.
- 530 Huggel, C., Salzmann, N., Allen, S., Caplan-Auerbach, J., Fischer, L., Haeberli, W., et al. (2010). Recent and future



- warm extreme events and high-mountain slope stability. *Philosophical Transactions of the Royal Society A: Mathematical, Physical and Engineering Sciences*, 368(1919), 2435–2459. <https://doi.org/10.1098/rsta.2010.0078>
- Hugonnet, R., McNabb, R., Berthier, E., Menounos, B., Nuth, C., Girod, L., Farinotti, D., Huss, M., Dussaillant, I., Brun, F., and Kääb, A.: Accelerated global glacier mass loss in the early twenty-first century, *Nature*, 592, <https://doi.org/10.1038/s41586-021-03436-z>, 2021.
- Huss, M.: Density assumptions for converting geodetic glacier volume change to mass change, *Cryosph.*, 7, 877–887, <https://doi.org/10.5194/tc-7-877-2013>, 2013.
- Huss, M. and Fischer, M.: Sensitivity of very small glaciers in the Swiss Alps to future climate change, <https://www.frontiersin.org/article/10.3389/feart.2016.00034>, 2016.
- Huss, M. and Hock, R.: Global-scale hydrological response to future glacier mass loss, *Nat Clim Chang*, 8, <https://doi.org/10.1038/s41558-017-0049-x>, 2018.
- Huss, M., Bookhagen, B., Huggel, C., Jacobsen, D., Bradley, R. S., Clague, J. J., et al. (2017). Toward mountains without permanent snow and ice. *Earth's Future*, 5(5), 418–435. <https://doi.org/https://doi.org/10.1002/2016EF000514>
- James, M.: Precision maps and 3-D uncertainty-based topographic change detection with structure-from-motion photogrammetry, 2017.
- Jiménez-Vaquero, C.: Cartografiado de la morfología subglaciar de La Maladeta y Aneto mediante georradar, Universitat Politècnica de València, 2016.
- Jomelli, V., Chapron, E., Favier, V., Rinterknecht, V., Braucher, R., Tournier, N., Gascoïn, S., Marti, R., Galop, D., Binet, S., Deschamps-Berger, C., Tissoux, H., Aumaitre, G., Bourlès, D. L., and Keddadouche, K.: Glacier fluctuations during the Late Glacial and Holocene on the Ariège valley, northern slope of the Pyrenees and reconstructed climatic conditions, *Mediterr. Geosci. Rev.*, 2, 37–51, <https://doi.org/10.1007/s42990-020-00018-5>, 2020.
- Kääb, A., Jacquemart, M., Gilbert, A., Leinss, S., Girod, L., Huggel, C., et al. (2021). Sudden large-volume detachments of low-angle mountain glaciers – more frequent than thought? *The Cryosphere*, 15(4), 1751–1785. <https://doi.org/10.5194/tc-15-1751-2021>
- Kellerer-Pirklbauer, A., Lieb, G. K., Avian, M., & Carrivick, J. (2012). climate change and rock fall events in high mountain areas: Numerous and extensive rock falls in 2007 at Mittlerer Burgstall, Central Austria. *Geografiska Annaler: Series A, Physical Geography*, 94(1), 59–78. <https://doi.org/https://doi.org/10.1111/j.1468-0459.2011.00449.x>
- Lampre Vitaller, F. (2003). *Monumentos Naturales de los Glaciares Pirenaicos*.
- Llena, M., Cavalli, M., Vericat, D., and Crema, S.: Assessing landscape changes associated to anthropic disturbances by means of the application of Structure from Motion photogrammetry using historical aerial imagery, *Rendiconti Online Societa Geologica Italiana*, 46, 74–81, <https://doi.org/10.3301/ROL.2018.55>, 2018.



Llena, M., Vericat, D., Martínez-Casasnovas, J. A., and Smith, M. W.: Geomorphic adjustments to multi-scale  
565 disturbances in a mountain river: A century of observations, *Catena* (Amst), 192, 104584,  
<https://doi.org/https://doi.org/10.1016/j.catena.2020.104584>, 2020.

López-Moreno, J. I.: Recent variations of snowpack depth in the central Spanish Pyrenees, *Arct Antarct Alp Res*, 37,  
253–260, [https://doi.org/10.1657/1523-0430\(2005\)037\[0253:RVOSDI\]2.0.CO;2](https://doi.org/10.1657/1523-0430(2005)037[0253:RVOSDI]2.0.CO;2), 2005.

López-Moreno, J. I., Nogués-Bravo, D., Chueca-Cía, J., and Julián-Andrés, A.: Change of topographic control on the  
570 extent of cirque glaciers since the Little Ice Age, *Geophys Res Lett*, 33, 1–5, <https://doi.org/10.1029/2006GL028204>, 2006.

López-Moreno, J. I., Alonso-González, E., Monserrat, O., del Río, L. M., Otero, J., Lapazaran, J., Luzi, G., Dematteis,  
N., Serreta, A., Rico, I., Serrano-Cañadas, E., Bartolomé, M., Moreno, A., Buisan, S., and Revuelto, J.: Ground-based remote-  
sensing techniques for diagnosis of the current state and recent evolution of the Monte Perdido Glacier, Spanish Pyrenees,  
*Journal of Glaciology*, 65, 85–100, <https://doi.org/10.1017/jog.2018.96>, 2019.

López-Moreno, J. I., García-Ruiz, J. M., Vicente-Serrano, S. M., Alonso-González, E., Revuelto-Benedí, J., Rico, I., et  
575 al. (2020). Critical discussion of: “A farewell to glaciers: Ecosystem services loss in the Spanish Pyrenees.” *Journal of  
Environmental Management*. <https://doi.org/10.1016/j.jenvman.2020.111247>

Marcer, M., Stenoft, P. A., Bjerre, E., Cimoli, E., Bjørk, A., Stenseng, L., and MacHguth, H.: Three decades of volume  
change of a small Greenlandic glacier using Ground Penetrating Radar, Structure from Motion, and Aerial Photogrammetry,  
580 *Arctic, Antarct. Alp. Res.*, 49, 411–425, <https://doi.org/10.1657/AAAR0016-049>, 2017.

Marti, R., Gascoïn, S., Houet, T., Ribière, O., Laffly, D., Condom, T., Monnier, S., Schmutz, M., Camerlynck, C.,  
Tihay, J. P., Soubeyroux, J. M., and René, P.: Evolution of Ossoue Glacier (French Pyrenees) since the end of the Little Ice  
Age, *Cryosphere*, 9, 1773–1795, <https://doi.org/10.5194/tc-9-1773-2015>, 2015.

Meier, M. F., Dyurgerov, M. B., Rick, U. K., O’Neel, S., Pfeffer, W. T., Anderson, R. S., et al. (2007). Glaciers  
585 Dominate Eustatic Sea-Level Rise in the 21st Century. *Science*, 317(5841), 1064–1067.  
<https://doi.org/10.1126/science.1143906>

Milner, A. M., Khamis, K., Battin, T. J., Brittain, J. E., Barrand, N. E., Füreder, L., et al. (2017). Glacier shrinkage  
driving global changes in downstream systems. *Proceedings of the National Academy of Sciences*, 114(37), 9770–9778.  
<https://doi.org/10.1073/pnas.1619807114>

Mölg, N. and Bolch, T.: Structure-from-Motion using historical aerial images to analyse changes in glacier surface  
590 elevation, *Remote Sens* (Basel), 9, <https://doi.org/10.3390/rs9101021>, 2017.

Oliva, M., Ruiz-Fernández, J., Barriendos, M., Benito, G., Cuadrat, J. M., Domínguez-Castro, F., García-Ruiz, J. M.,  
Giralt, S., Gómez-Ortiz, A., Hernández, A., López-Costas, O., López-Moreno, J. I., López-Sáez, J. A., Martínez-Cortizas, A.,  
Moreno, A., Prohom, M., Saz, M. A., Serrano, E., Tejedor, E., Trigo, R., Valero-Garcés, B., and Vicente-Serrano, S. M.: The  
595 Little Ice Age in Iberian mountains, *Earth Sci Rev*, 177, 175–208,  
<https://doi.org/https://doi.org/10.1016/j.earscirev.2017.11.010>, 2018.



- Otero García, J.: Generación automática de malla de elementos finitos en modelos evolutivos de dinámica de glaciares, Universidad Politécnica de Madrid, Madrid, 2008.
- Otto, J.-C.: Proglacial lakes in high mountain environments, 231–247, [https://doi.org/10.1007/978-3-319-94184-4\\_14](https://doi.org/10.1007/978-3-319-94184-4_14), 2019.
- 600 Pastor Argüello, F.: determinación del balance anual de masa y movimiento del hielo en el glaciar de la Maladeta. Año hidrológico 2012–2013, 68, 2013.
- Pepin, N., Bradley, R. S., Diaz, H. F., Baraer, M., Caceres, E. B., Forsythe, N., et al. (2015). Elevation-dependent warming in mountain regions of the world. *Nature Climate Change*, 5(5), 424–430. <https://doi.org/10.1038/nclimate2563>
- Procházková, B., Engel, Z., and Tomíček, J.: Geometric changes of three glaciers in Dickson Land, central Spitsbergen, 605 during the period 1990–2015, *Polar Sci.*, 20, 129–135, <https://doi.org/https://doi.org/10.1016/j.polar.2019.05.004>, 2019.
- de Reu, J., Bourgeois, J., Bats, M., Zwertvaegher, A., Gelorini, V., de Smedt, P., Chu, W., Antrop, M., de Maeyer, P., Finke, P., van Meirvenne, M., Verniers, J., and Crombé, P.: Application of the topographic position index to heterogeneous landscapes, *Geomorphology*, 186, 39–49, <https://doi.org/https://doi.org/10.1016/j.geomorph.2012.12.015>, 2013.
- Rabatel, A., Francou, B., Soruco, A., Gomez, J., Cáceres, B., Ceballos, J. L., et al. (2013). Current state of glaciers in 610 the tropical Andes: a multi-century perspective on glacier evolution and climate change. *The Cryosphere*, 7(1), 81–102. <https://doi.org/10.5194/tc-7-81-2013>
- Rajendra, Y. D., Mehrotra, S. C., Kale, K. V., Manza, R. R., Dhumal, R. K., Nagne, A. D., and Vibhute, A. D.: Evaluation of partially overlapping 3D point cloud's registration by using ICP variant and cloudcompare, *Int. Arch. Photogramm. Remote Sens. Spat. Inf. Sci. - ISPRS Arch.*, XL–8, 891–897, [https://doi.org/10.5194/isprsarchives-XL-8-891-](https://doi.org/10.5194/isprsarchives-XL-8-891-2014) 615 2014, 2014.
- Rico, I., Izagirre, E., Serrano, E., and López-Moreno, J. I.: Superficie glaciar actual en los Pirineos: Una actualización para 2016, *Pirineos*, 172, e029, <https://doi.org/10.3989/Pirineos.2017.172004>, 2017.
- Rico, I., Magnin, F., López Moreno, J. I., Serrano, E., Alonso-González, E., Revuelto, J., et al. (2021). First evidence of rock wall permafrost in the Pyrenees (Vignemale peak, 3,298 m a.s.l., 42°46'16"N/0°08'33"W). *Permafrost and Periglacial Processes*, 32(4), 673–680. <https://doi.org/https://doi.org/10.1002/ppp.2130>
- 620 Riihimäki, C. A., MacGregor, K. R., Anderson, R. S., Anderson, S. P., & Loso, M. G. (2005). Sediment evacuation and glacial erosion rates at a small alpine glacier. *Journal of Geophysical Research: Earth Surface*, 110(F3). <https://doi.org/https://doi.org/10.1029/2004JF000189>
- Shaw, T. E., Ulloa, G., Farías-Barahona, D., Fernandez, R., Lattus, J. M., and McPhee, J.: Glacier albedo reduction and 625 drought effects in the extratropical Andes, 1986–2020, *J. Glaciol.*, 67, 158–169, [https://doi.org/DOI: 10.1017/jog.2020.102](https://doi.org/DOI:10.1017/jog.2020.102), 2021.
- Shugar, D. H., Burr, A., Haritashya, U. K., Kargel, J. S., Watson, C. S., Kennedy, M. C., Bevington, A. R., Betts, R. A., Harrison, S., and Strattman, K.: Rapid worldwide growth of glacial lakes since 1990, *Nat Clim Chang*, 10, 939–945, <https://doi.org/10.1038/s41558-020-0855-4>, 2020.





- 630 Snavely, N., Seitz, S. M., and Szeliski, R.: Photo tourism: exploring photo collections in 3D, *ACM Trans. Graph.*, 25, 835–846, <https://doi.org/10.1145/1141911.1141964>, 2006.
- Snook, D. L., & Milner, A. M. (2001). The influence of glacial runoff on stream macroinvertebrate communities in the Taillon catchment, French Pyrénées. *Freshwater Biology*, 46(12), 1609–1623. <https://doi.org/https://doi.org/10.1046/j.1365-2427.2001.00848.x>
- 635 Solomina, O. N., Bradley, R. S., Jomelli, V., Geirsdottir, A., Kaufman, D. S., Koch, J., McKay, N. P., Masiokas, M., Miller, G., Nesje, A., Nicolussi, K., Owen, L. A., Putnam, A. E., Wanner, H., Wiles, G., and Yang, B.: Glacier fluctuations during the past 2000 years, <https://doi.org/10.1016/j.quascirev.2016.04.008>, 2016.
- Vidaller, I., Revuelto, J., Izagirre, E., Rojas-Heredia, F., Alonso-González, E., Gascoïn, S., René, P., Berthier, E., Rico, I., Moreno, A., Serrano, E., Serreta, A., and López-Moreno, J. I.: Toward an ice-free mountain range: Demise of Pyrenean  
640 glaciers during 2011–2020, *Geophys Res Lett*, 48, <https://doi.org/10.1029/2021GL094339>, 2021.
- Vuille, M., Francou, B., Wagnon, P., Juen, I., Kaser, G., Mark, B. G., & Bradley, R. S. (2008). Climate change and tropical Andean glaciers: Past, present and future. *Earth-Science Reviews*, 89(3), 79–96. <https://doi.org/https://doi.org/10.1016/j.earscirev.2008.04.002>
- Yao, X., Liu, S., Han, L., Sun, M., and Zhao, L.: Definition and classification system of glacial lake for inventory and  
645 hazards study, *Journal of Geographical Sciences*, 28, 193–205, <https://doi.org/10.1007/s11442-018-1467-z>, 2018.
- Yue, X., Li, Z., Zhao, J., Fan, J., Takeuchi, N., and Wang, L.: Variation in albedo and its relationship with surface dust at Urumqi Glacier No. 1 in Tien Shan, China, <https://www.frontiersin.org/articles/10.3389/feart.2020.00110>, 2020.
- Zemp, M., Frey, H., Gärtner-Roer, I., Nussbaumer, S. U., Hoelzle, M., Paul, F., Haeberli, W., Denzinger, F., Ahlstrøm, A. P., Anderson, B., Bajracharya, S., Baroni, C., Braun, L. N., Càceres, B. E., Casassa, G., Cobos, G., Dàvila, L. R., Delgado  
650 Granados, H., Demuth, M. N., Espizua, L., Fischer, A., Fujita, K., Gadek, B., Ghazanfar, A., Hagen, J. O., Holmlund, P., Karimi, N., Li, Z., Pelto, M., Pitte, P., Popovnin, V. V., Portocarrero, C. A., Prinz, R., Sangewar, C. V., Severskiy, I., Sigurdsson, O., Soruco, A., Usabaliev, R., and Vincent, C.: Historically unprecedented global glacier decline in the early 21st century, *Journal of Glaciology*, 61, 745–762, <https://doi.org/10.3189/2015JoG15J017>, 2015.